Published in final edited form as:
Magn Reson Med. 2012 September ; 68(3): 868–873. doi:10.1002/mrm.23287.

Diffusion-Prepared Fast Imaging with Steady-State Free Precession (DP-FISP): A Rapid Diffusion MRI Technique at 7T

Lan Lu[1], **Bernadette Erokwu**[1], **Gregory Lee**[1], **Vikas Gulani**[1,2], **Mark A. Griswold**[1,2], **Katherine M. Dell**[3,4], and **Chris A. Flask**[1,2]

[1]Department of Radiology, Case Western Reserve University, Cleveland, OH 44106

[2]Department of Biomedical Engineering, Case Western Reserve University, Cleveland, OH 44106

[3]CWRU Center for the Study of Kidney Disease and Biology, MetroHealth Campus, Case Western Reserve University, Cleveland, OH 44109

[4]Department of Pediatrics, Case Western Reserve University, Cleveland, OH 44106

Abstract

Diffusion MRI is a useful imaging technique with many clinical applications. Many diffusion MRI studies have utilized Echo-Planar Imaging (EPI) acquisition techniques. In this study, we have developed a rapid Diffusion Prepared - Fast Imaging with Steady-State Free Precession (DP-FISP) MRI acquisition for a preclinical 7T scanner providing diffusion-weighted images in less than 500 ms and DTI assessments in approximately 1 minute with minimal image artifacts in comparison to EPI. Phantom Apparent Diffusion Coefficient (ADC) and Fractional Anisotropy (FA) assessments obtained from the DP-FISP acquisition resulted in good agreement with EPI and spin echo diffusion methods. The mean ADC was 2.0×10^{-3} mm^2/s, 1.90×10^{-3} mm^2/s and 1.97×10^{-3} mm^2/s for DP-FISP, DW-SE and DW-EPI, respectively. The mean FA was 0.073, 0.072, and 0.070 for DP-FISP, DW-SE and DW-EPI, respectively. Initial *in vivo* studies show reasonable ADC values in a normal mouse brain and polycystic rat kidneys.

Keywords

diffusion; MRI; FISP; 7T

INTRODUCTION

Diffusion MRI has proven to be an extremely useful imaging technique with clinical applications in assessments of stroke (1,2), neurodegenerative disease (3,4), cancer (5–7), kidney disease (8,9), and liver disease (10,11). A key advantage of Diffusion MRI is its ability to provide reliable quantitative assessments of tissues, which enables both early-stage disease detection as well as an opportunity for longitudinal assessments of disease progression. In addition, a variety of Diffusion MRI techniques, such as Diffusion Tensor Imaging (DTI) and Intra-Voxel Incoherent Motion (IVIM), have been developed to study the effects of tissue anisotropy and perfusion, respectively (12–16).

The large majority of Diffusion MRI studies have utilized Echo-Planar Imaging (EPI) acquisition techniques in order to rapidly acquire diffusion-weighted images. However, EPI

Corresponding author: Chris A. Flask, Ph.D., Assistant Professor of Radiology and Biomedical Engineering, Case Western Reserve University, University Hospitals of Cleveland, 11100 Euclid Avenue, Bolwell Building, Room B115, Cleveland, OH 44106, PH: 216-844-4963, Fax: 216-844-4987, chris.flask@uhhospitals.org.

techniques are susceptible to off-resonance distortion artifacts (17). Importantly, these artifacts are greatly increased on high field human and small animal MRI scanners making EPI acquisitions extremely problematic, especially for body imaging applications. At the same time, conventional spin echo Diffusion MRI acquisitions can require excessively long acquisition times. Therefore, a need exists to develop a robust and rapid Diffusion MRI protocol for high field MRI scanners.

A variety of alternative acquisition strategies to EPI have been applied to improve overall image quality in diffusion MRI applications. Multi-echo spin echo acquisitions maintain the acquisition speed and greatly limit the off-resonance artifacts of EPI acquisitions (18). However, quantification errors can be generated from the effects of Magnetization Transfer and T2 decay (19–21). Steady-state diffusion weighted imaging techniques have also been developed that combine a conventional diffusion preparation scheme with a steady-state imaging readout train, such as low flip angle RARE (22), FLASH (23,24), and Balanced SSFP (25). However, in some of these methods, a significant delay (~100 ms) between the end of the diffusion preparation and the acquisition of the central region of k-space exists because of the approach to steady state and / or non-centric k-space trajectories. This delay can result in loss of diffusion sensitivity and therefore significant diffusion quantification errors. In addition, most of the techniques used non-slice selective preparation, making multislice 2D acquisitions less time-efficient. Another rapid diffusion technique applied the diffusion gradients directly within an SSFP acquisition (26,27). While highly time-efficient, the diffusion sensitivity is much more complicated and is dependent on flip angle, T1, and T2. In addition, at 7T, balanced SSFP acquisitions may exhibit banding artifacts.

Here, we describe initial *in vitro* and *in vivo* results from a Diffusion-Prepared Fast Imaging with Steady-State Free Precession (DP-FISP) MRI acquisition technique implemented on a 7T small animal MRI scanner. This technique combines a conventional 90_x-180_y-90_{-x} diffusion preparation scheme with a single-shot, centrically-encoded FISP acquisition to provide diffusion-weighted images in < 500 ms. In this initial report, we quantitatively validated the DP-FISP technique against conventional EPI and spin echo acquisitions in both phantom and *in vivo* rodent brain and kidney experiments.

MATERIALS AND METHODS

DP-FISP Pulse Sequence Design

All acquisitions were implemented on a Bruker Biospec 7T MRI scanner (Billerica, MA) equipped with a 400 mT/m gradient insert. The DP-FISP pulse sequence was developed by combining a slice-selective diffusion preparation (90_x-180_y-90_{-x}) with a single-shot, centrically-encoded FISP imaging readout (Fig. 1). The diffusion preparation was designed with bipolar diffusion gradients to limit cardiac and respiratory motion artifacts. A slice-selective diffusion preparation was used to enable eventual interleaved, multislice DP-FISP acquisitions (Hermite excitation pulses, t_{rf} = 1 ms). The slice thickness of the diffusion preparation was set to 3 times that of the FISP imaging readout as in this initial study to ensure accurate diffusion preparation in the imaging slice. The accuracy of this slice thickness ratio was validated with B_1 calibration assessments (data not shown) and was shown previously to aid in T2 relaxation assessments(28). Gradient spoilers were applied after the diffusion preparation to avoid spurious echoes. The FISP imaging readout was described previously and provides *in vivo* images in <500 ms with relatively high SNR and minimal off-resonance distortion and ghosting artifacts in comparison to EPI (29). The FISP imaging readout was designed with centric encoding to retain maximal diffusion weighted contrast from the diffusion preparation. The FISP imaging readout was also utilized to prevent banding artifacts typical of balanced SSFP acquisitions on high field MRI scanners.

Quantitative Phantom Validation of DP-FISP Diffusion Assessments

To quantitatively verify the DP-FISP technique, DTI images (six directions (b = 450 s/mm^2) + null (b = 0 s/mm^2), Δ = 12 ms, δ = 6 ms) of a cylindrical water phantom were obtained to compare with a conventional diffusion weighted spin echo (DW-SE) and DW-EPI acquisitions. The DP-FISP acquisition parameters were TR / TE = 2.6 ms / 1.3 ms, α = 60°, matrix = 128×128, resolution = 0.31×0.31 mm, imaging slice thickness = 2 mm. The overall duration for the diffusion preparation was 36 ms. A scan delay of 8 seconds was applied between scans and two b = 0 s/mm^2 scans were incorporated to limit the effects of T1 relaxation. Identical diffusion parameters and acquisition geometry were used for both the DW-SE and DW-EPI acquisitions. For the DW-SE method, the TR / TE were set to 8,000 ms / 20 ms, to limit the effects of T1 and T2 relaxation. The single-shot DW-EPI acquisition used an echo time of 100 ms and the same scan repetition time as the DP-FISP acquisition (8 seconds). The phantom images were acquired with 16 averages for both DP-FISP and DW-EPI methods (total acquisition time = 17 min each), while 1 average for DW-SE method (total acquisition time = 120 min).

All images were exported and processed off-line using in-house Matlab software (The Mathworks, Natick, MA). ADC and FA maps were calculated on a pixel by pixel basis using established methods (30,31). Mean ADC and FA were calculated for each phantom image using an ROI analysis. All imaging acquisitions were repeated 5 times and a two-tailed student's t-test was then used to compare the mean ADC and FA from each acquisition.

Initial *In vivo* DP-FISP Evaluation

The DP-FISP technique was further evaluated by obtaining diffusion weighted images and associated ADC map of a mouse brain (C57BL6/J, Jackson Labs) and rat kidneys (PCK rat model of Autosomal Recessive Polycystic Kidney Disease,(32)). All animal studies were conducted in accordance with established protocols approved by the Institutional Animal Care and Use Committee of Case Western Reserve University. Animals were initially anesthetized with 2% isoflurane in O_2 and then mounted in an appropriate transmit/receive volume coil for imaging (mouse = 35mm ID, rat = 72mm ID). Animals were maintained at 34±1°C and 30–60 breaths / minute using warm air and adjustable isoflurane levels, respectively.

The DP-FISP acquisition (TR/TE = 2.6 / 1.3 ms, α=60°, matrix = 128×128, resolution = 0.31×0.31 mm, imaging slice thickness = 2 mm, diffusion preparation slice thickness = 6 mm, 6 diffusion directions + null, b = 0 and 450 s/ mm^2, Δ/δ = 8.5 / 4 ms) was used to obtain DTI measurements of a normal mouse brain (4-month old, C57B6/J mouse). The total duration of the diffusion preparation was 28 ms. A delay of eight seconds was again applied to minimize T1 relaxation effects between consecutive scans. One axial slice with four averages was acquired for the C57BL6/J mouse. The total data acquisition time was approximately 4 minutes with prospective respiration gating. For comparison, the DW-SE method (TR / TE = 2,000 ms / 20 ms) was also used to acquire DTI data on the same animal and imaging slice with a total scan time of 40 min for one average with respiratory gating.

In vivo DTI measurements were also obtained on the kidneys of a 2-month-old PCK rat. DTI data were acquired using the DP-FISP method similar to the mouse brain DTI study above (TR/TE = 3.3 / 1.65 ms, α=60°, matrix = 256×128, resolution = 0.55 × 0.55 mm, imaging slice thickness = 2 mm, diffusion preparation slice thickness = 6 mm, null + 6 diffusion directions, b = 0 and 340 s/ mm^2, Δ/δ = 7.5 / 3 ms). The total duration of the diffusion preparation was 22 ms. These *in vivo* kidney DTI results were obtained with one signal average requiring approximately one minute with respiratory gating. Note that DW-

SE imaging data were not acquired for this renal imaging application due to excessive respiratory motion artifacts.

RESULTS

Representation phantom diffusion weighted images (b = 0 and b = 450 s/mm^2) and quantitative ADC and FA maps from DP-FISP, DW-SE, and DW-EPI techniques are shown in Fig. 2. Similar images and ADC / FA maps were obtained between the three different methods. Mean values of each diffusion parameter from five repeated measurements for each acquisition scheme are shown in Table 1. Importantly, the mean ADC and FA from the DP-FISP acquisition (17 min. acq. time) were consistent with both conventional DW-SE (120 min. acq. time) and DW-EPI (17 min. acq. time) acquisitions. No statistical difference in ADC was observed between the DP-FISP and DW-EPI acquisitions (2.00 ± 0.06 mm^2/s vs. 1.97 ± 0.04 mm^2/s, respectively, $p = 0.2$). The mean ADC values for the DP-FISP and DW-EPI acquisitions were ~5% higher than for the DW-SE acquisition (1.90 ADC ± 0.06 mm^2/s) and were significantly different ($p < 0.05$). No statistic difference in FA values was observed all three methods ($p > 0.3$).

Figure 3 shows representative diffusion weighted images and corresponding ADC maps of a normal mouse brain acquired with a DP-FISP acquisition (4 min. acq. time, 4 averages) and a DW-SE acquisition (40 min. acq. time, 1 average). Despite the different image contrast obtained with the FISP and SE imaging readouts, the ADC maps (color overlay) were remarkably consistent between the two methods. The mean ADC values were calculated in two different regions: CSF and gray/white matter. For the CSF ROIs, the mean ADC for the DP-FISP and DW-SE acquisitions were $1.57\pm0.25\times10^{-3}$ mm^2/s and $1.51\pm0.40\times10^{-3}$ mm^2/s, respectively. The mean ADC for the gray/white matter for DP-FISP and DW-SE acquisitions were $0.87\pm0.12\times10^{-3}$ mm^2/s and $0.82\pm0.13\times10^{-3}$ mm^2/s, respectively. Note that these results were obtained with a 10-fold reduction in overall acquisition time.

In order to assess the sensitivity of the DP-FISP technique to known pathology, diffusion weighted images and an overlaid ADC map of polycystic rat kidneys are shown in Fig. 4. These images and corresponding ADC maps were obtained with a single signal average (total acquisition time ~1 min with prospective respiratory gating). The mean ADC for left and right kidneys was 2.55×10^{-3} mm^2/s and 2.31×10^{-3} mm^2/s, respectively. The DP-FISP images (Fig. 4) clearly demonstrate the distinctly brighter appearance of the corticomedullary cysts (hyperintense regions). These cysts also exhibit increased ADC values (yellow regions) due to reduced diffusion restrictions as shown in previous reports (33).

DISCUSSION

In this study, initial *in vitro* and *in vivo* diffusion MRI results were obtained using a rapid and quantitatively accurate DP-FISP acquisition on a 7T small animal MRI scanner. The DP-FISP technique combines a slice-selective diffusion preparation followed by a centrically-encoded FISP imaging readout to provide diffusion MRI data with minimal image artifacts in comparison to conventional EPI acquisitions and very short acquisition time in comparison to diffusion weighted spin echo acquisitions.

There are several important design features of the DP-FISP acquisition. Most importantly, the FISP imaging readout is applied with centric k-space encoding. This approach minimizes the time delay between the end of the diffusion preparation and the acquisition of the central region of k-space. In this way, the loss of diffusion sensitivity caused by T1 relaxation recovery is also minimized. A FISP imaging readout was selected for this study instead of a

balanced SSFP readout primarily to limit well-known banding artifacts which are increased on high field MRI scanners. An alternative approach using balanced SSFP would be to acquire multiple images with different RF phase variation sequences to reconstruct banding free images (34). However, this approach would require multiple acquisitions in order to correct banding artifacts.

Phantom diffusion MRI studies were conducted to quantitatively validate the DP-FISP method with conventional DW-EPI and DW-SE techniques. The DP-FISP acquisition exhibited nearly identical mean phantom ADC and FA values in comparison to a conventional DW-EPI acquisition. The mean phantom ADC values for the both DP-FISP and DW-EPI acquisitions were both ~5% higher than for the DW-SE acquisition. Interestingly, this small difference in ADC values was also observed in the initial *in vivo* mouse brain results measuring the ADC of both CSF and normal mouse brain tissue (see discussion of *in vivo* results below). This difference is most likely due to slight underestimation of the effective b-value for the DP-FISP acquisition by not accounting for the gradient pulses and relaxation effects during the 5 'dummy' scans and in the initial central k-space lines. Despite these small differences in ADC, these results do suggest that the DP-FISP acquisition may provide accurate diffusion assessments similar to conventional DW-SE with a ~10 fold reduction in acquisition time.

Initial *in vivo* diffusion studies demonstrated that the DP-FISP technique provides quantitatively similar results with conventional DW-SE in a mouse brain (Fig. 3). The mouse brain ADC maps and mean values of CSF / normal brain tissue were consistent between these two methods and were also consistent with previous studies (35,36). The DP-FISP imaging data were obtained with 4 signal averages resulting in an acquisition time of only 4 minutes with a long scan repetition time (~8 seconds) to limit T1 relaxation effects. DP-FISP diffusion data were also obtained from the PCK rat kidneys (Fig. 4). The measured ADC values for the non-cystic regions of the PCK rat kidneys (red regions) were consistent with previous kidney diffusion MRI studies (8,37). In addition, the ADC map delineates the corticomedullary cysts (arrows) demonstrating the sensitivity of the DP-FISP technique to known pathophysiologic structures(33). While these initial *in vivo* DP-FISP images were acquired with modest b-values, higher b-value acquisition (ex. 1000 s/mm^2) can be obtained by simply increasing the duration of the diffusion preparation.

Overall, the advantages of the DP-FISP technique are its short acquisition time and minimal image artifacts in comparison to EPI, especially for high field MRI scanners where EPI off-resonance distortion and ghosting artifacts are extremely problematic. Therefore, specialized shimming, segmented acquisitions, and/or image reconstructions are not required by DP-FISP to obtain useful and quantitative diffusion data. Due to its short acquisition time, the DP-FISP technique can be used to obtain diffusion weighted images within a single respiratory cycle for rodents which can reduce respiratory motion artifacts in comparison to DW-SE or segmented DW-EPI acquisitions.

The DP-FISP technique, as presented here, also has several important limitations. First, the diffusion preparation schema requires the thickness of the diffusion preparation slab to be three times larger than the imaging readout. This initial design would extend the time to acquire multislice 2D diffusion data as adjacent slices would have to be acquired in a separate DP-FISP scan. One simple approach to overcome this limitation would be to optimize the excitation profile of the diffusion preparation pulses which could reduce the diffusion slab to imaging slice thickness ratio closer to 1. An alternative approach would be to investigate the utility of a centric 3D FISP readout. An additional limitation of the FISP imaging readout is the typically decreased SNR relative to conventional spin echo acquisitions. Fortunately, the SNR/time of the FISP acquisition is higher than for a spin echo

acquisition which results in a ~10-fold reduction in acquisition time while still obtaining nearly identical ADC and FA results. In addition, we have shown here that useful *in vivo* diffusion MRI results can be obtained from a single signal average despite the overall decrease in SNR (Figure 4).

In conclusion, this study reports a rapid and quantitatively accurate diffusion MRI technique, DP-FISP, for high field MRI scanners. It combines a diffusion preparation with a rapid FISP imaging readout to provide diffusion-weighted images in less than 500 ms, and DTI data in approximately 1 minute with minimal image artifacts in comparison to DW-EPI. DP-FISP was quantitatively validated against conventional DW-EPI and DW-SE acquisitions in both phantom and *in vivo* studies of normal and diseased organs. This new technique provides an alternative method for many diffusion imaging applications on high field MRI scanners where off-resonance artifacts can severely limit the use of EPI acquisitions.

Acknowledgments

The authors would like to acknowledge the support of NIH/NIDDK RO1 DK085099-01, the Case Comprehensive Cancer Center (P30 CA43703), and the Cystic Fibrosis Center (P30 DK027651).

REFERENCES

1. Schlaug G, Siewert B, Benfield A, Edelman RR, Warach S. Time course of the apparent diffusion coefficient (ADC) abnormality in human stroke. Neurology. 1997; 49(1):113–119. [PubMed: 9222178]
2. Warach S, Gaa J, Siewert B, Wielopolski P, Edelman RR. Acute human stroke studied by whole brain echo planar diffusion-weighted magnetic resonance imaging. Ann Neurol. 1995; 37(2):231–241. [PubMed: 7847864]
3. Rosas HD, Tuch DS, Hevelone ND, Zaleta AK, Vangel M, Hersch SM, Salat DH. Diffusion tensor imaging in presymptomatic and early Huntington's disease: Selective white matter pathology and its relationship to clinical measures. Mov Disord. 2006; 21(9):1317–1325. [PubMed: 16755582]
4. Taoka T, Iwasaki S, Sakamoto M, Nakagawa H, Fukusumi A, Myochin K, Hirohashi S, Hoshida T, Kichikawa K. Diffusion anisotropy and diffusivity of white matter tracts within the temporal stem in Alzheimer disease: evaluation of the "tract of interest" by diffusion tensor tractography. AJNR Am J Neuroradiol. 2006; 27(5):1040–1045. [PubMed: 16687540]
5. Koh DM, Collins DJ. Diffusion-weighted MRI in the body: applications and challenges in oncology. AJR Am J Roentgenol. 2007; 188(6):1622–1635. [PubMed: 17515386]
6. Padhani AR, Liu G, Koh DM, Chenevert TL, Thoeny HC, Takahara T, Dzik-Jurasz A, Ross BD, Van Cauteren M, Collins D, Hammoud DA, Rustin GJ, Taouli B, Choyke PL. Diffusion-weighted magnetic resonance imaging as a cancer biomarker: consensus and recommendations. Neoplasia. 2009; 11(2):102–125. [PubMed: 19186405]
7. Patterson DM, Padhani AR, Collins DJ. Technology insight: water diffusion MRI--a potential new biomarker of response to cancer therapy. Nat Clin Pract Oncol. 2008; 5(4):220–233. [PubMed: 18301415]
8. Ries M, Jones RA, Basseau F, Moonen CT, Grenier N. Diffusion tensor MRI of the human kidney. J Magn Reson Imaging. 2001; 14(1):42–49. [PubMed: 11436213]
9. Thoeny HC, De Keyzer F, Oyen RH, Peeters RR. Diffusion-weighted MR imaging of kidneys in healthy volunteers and patients with parenchymal diseases: initial experience. Radiology. 2005; 235(3):911–917. [PubMed: 15845792]
10. Taouli B, Tolia AJ, Losada M, Babb JS, Chan ES, Bannan MA, Tobias H. Diffusion-weighted MRI for quantification of liver fibrosis: preliminary experience. AJR Am J Roentgenol. 2007; 189(4):799–806. [PubMed: 17885048]

11. Taouli B, Vilgrain V, Dumont E, Daire JL, Fan B, Menu Y. Evaluation of liver diffusion isotropy and characterization of focal hepatic lesions with two single-shot echo-planar MR imaging sequences: prospective study in 66 patients. Radiology. 2003; 226(1):71–78. [PubMed: 12511671]
12. Le Bihan D, Breton E, Lallemand D, Aubin ML, Vignaud J, Laval-Jeantet M. Separation of diffusion and perfusion in intravoxel incoherent motion MR imaging. Radiology. 1988; 168(2): 497–505. [PubMed: 3393671]
13. Luciani A, Vignaud A, Cavet M, Nhieu JT, Mallat A, Ruel L, Laurent A, Deux JF, Brugieres P, Rahmouni A. Liver cirrhosis: intravoxel incoherent motion MR imaging--pilot study. Radiology. 2008; 249(3):891–899. [PubMed: 19011186]
14. Mukherjee P, McKinstry RC. Reversible posterior leukoencephalopathy syndrome: evaluation with diffusion-tensor MR imaging. Radiology. 2001; 219(3):756–765. [PubMed: 11376265]
15. Pierpaoli C, Jezzard P, Basser PJ, Barnett A, Di Chiro G. Diffusion tensor MR imaging of the human brain. Radiology. 1996; 201(3):637–648. [PubMed: 8939209]
16. Wu MT, Tseng WY, Su MY, Liu CP, Chiou KR, Wedeen VJ, Reese TG, Yang CF. Diffusion tensor magnetic resonance imaging mapping the fiber architecture remodeling in human myocardium after infarction: correlation with viability and wall motion. Circulation. 2006; 114(10):1036–1045. [PubMed: 16940196]
17. Jezzard P, Barnett AS, Pierpaoli C. Characterization of and correction for eddy current artifacts in echo planar diffusion imaging. Magn Reson Med. 1998; 39(5):801–812. [PubMed: 9581612]
18. Kinoshita T, Yashiro N, Ihara N, Funatu H, Fukuma E, Narita M. Diffusion-weighted half-Fourier single-shot turbo spin echo imaging in breast tumors: differentiation of invasive ductal carcinoma from fibroadenoma. J Comput Assist Tomogr. 2002; 26(6):1042–1046. [PubMed: 12488758]
19. Outwater EK, Mitchell DG, Vinitski S. Abdominal MR imaging: evaluation of a fast spin-echo sequence. Radiology. 1994; 190(2):425–429. [PubMed: 8284393]
20. Deng J, Miller FH, Salem R, Omary RA, Larson AC. Multishot diffusion-weighted PROPELLER magnetic resonance imaging of the abdomen. Invest Radiol. 2006; 41(10):769–775. [PubMed: 16971801]
21. Pipe JG, Farthing VG, Forbes KP. Multishot diffusion-weighted FSE using PROPELLER MRI. Magn Reson Med. 2002; 47(1):42–52. [PubMed: 11754441]
22. Norris DG, Bornert P, Reese T, Leibfritz D. On the application of ultra-fast RARE experiments. Magn Reson Med. 1992; 27(1):142–164. [PubMed: 1435200]
23. Sinha U, Sinha S. High speed diffusion imaging in the presence of eddy currents. J Magn Reson Imaging. 1996; 6(4):657–666. [PubMed: 8835960]
24. Thomas DL, Pell GS, Lythgoe MF, Gadian DG, Ordidge RJ. A quantitative method for fast diffusion imaging using magnetization-prepared TurboFLASH. Magn Reson Med. 1998; 39(6): 950–960. [PubMed: 9621919]
25. Jeong EK, Kim SE, Parker DL. High-resolution diffusion-weighted 3D MRI using diffusion-weighted driven-equilibrium (DW-DE) and multishot segmented 3D-SSFP without navigator echoes. Magn Reson Med. 2003; 50(4):821–829. [PubMed: 14523969]
26. Le Bihan D. Intravoxel incoherent motion imaging using steady-state free precession. Magn Reson Med. 1988; 7(3):346–351. [PubMed: 3205150]
27. McNab JA, Miller KL. Sensitivity of diffusion weighted steady state free precession to anisotropic diffusion. Magn Reson Med. 2008; 60(2):405–413. [PubMed: 18666106]
28. Pell GS, Briellmann RS, Waites AB, Abbott DF, Lewis DP, Jackson GD. Optimized clinical T2 relaxometry with a standard CPMG sequence. J Magn Reson Imaging. 2006; 23(2):248–252. [PubMed: 16416434]
29. Shah T, Lu L, Dell KM, Pagel MD, Griswold MA, Flask CA. CEST-FISP: a novel technique for rapid chemical exchange saturation transfer MRI at 7 T. Magn Reson Med. 2011; 65(2):432–437. [PubMed: 20939092]
30. Basser PJ, Pierpaoli C. A simplified method to measure the diffusion tensor from seven MR images. Magn Reson Med. 1998; 39(6):928–934. [PubMed: 9621916]
31. Mukherjee P, Berman JI, Chung SW, Hess CP, Henry RG. Diffusion tensor MR imaging and fiber tractography: theoretic underpinnings. AJNR Am J Neuroradiol. 2008; 29(4):632–641. [PubMed: 18339720]

32. Goto M, Hoxha N, Osman R, Dell KM. The renin-angiotensin system and hypertension in autosomal recessive polycystic kidney disease. Pediatr Nephrol. 2010; 25(12):2449–2457. [PubMed: 20798958]

33. Zhang JL, Sigmund EE, Chandarana H, Rusinek H, Chen Q, Vivier PH, Taouli B, Lee VS. Variability of renal apparent diffusion coefficients: limitations of the monoexponential model for diffusion quantification. Radiology. 254(3):783–792. [PubMed: 20089719]

34. Bangerter NK, Hargreaves BA, Vasanawala SS, Pauly JM, Gold GE, Nishimura DG. Analysis of multiple-acquisition SSFP. Magn Reson Med. 2004; 51(5):1038–1047. [PubMed: 15122688]

35. Chahboune H, Ment LR, Stewart WB, Ma X, Rothman DL, Hyder F. Neurodevelopment of C57B/L6 mouse brain assessed by in vivo diffusion tensor imaging. NMR Biomed. 2007; 20(3):375–382. [PubMed: 17451176]

36. Rau PR, Sellner J, Heiland S, Plaschke K, Schellinger PD, Meyding-Lamade UK, Lamade WR. Apparent diffusion coefficient in the aging mouse brain: a magnetic resonance imaging study. Life Sci. 2006; 78(11):1175–1180. [PubMed: 16213530]

37. Notohamiprodjo M, Glaser C, Herrmann KA, Dietrich O, Attenberger UI, Reiser MF, Schoenberg SO, Michaely HJ. Diffusion tensor imaging of the kidney with parallel imaging: initial clinical experience. Invest Radiol. 2008; 43(10):677–685. [PubMed: 18791409]

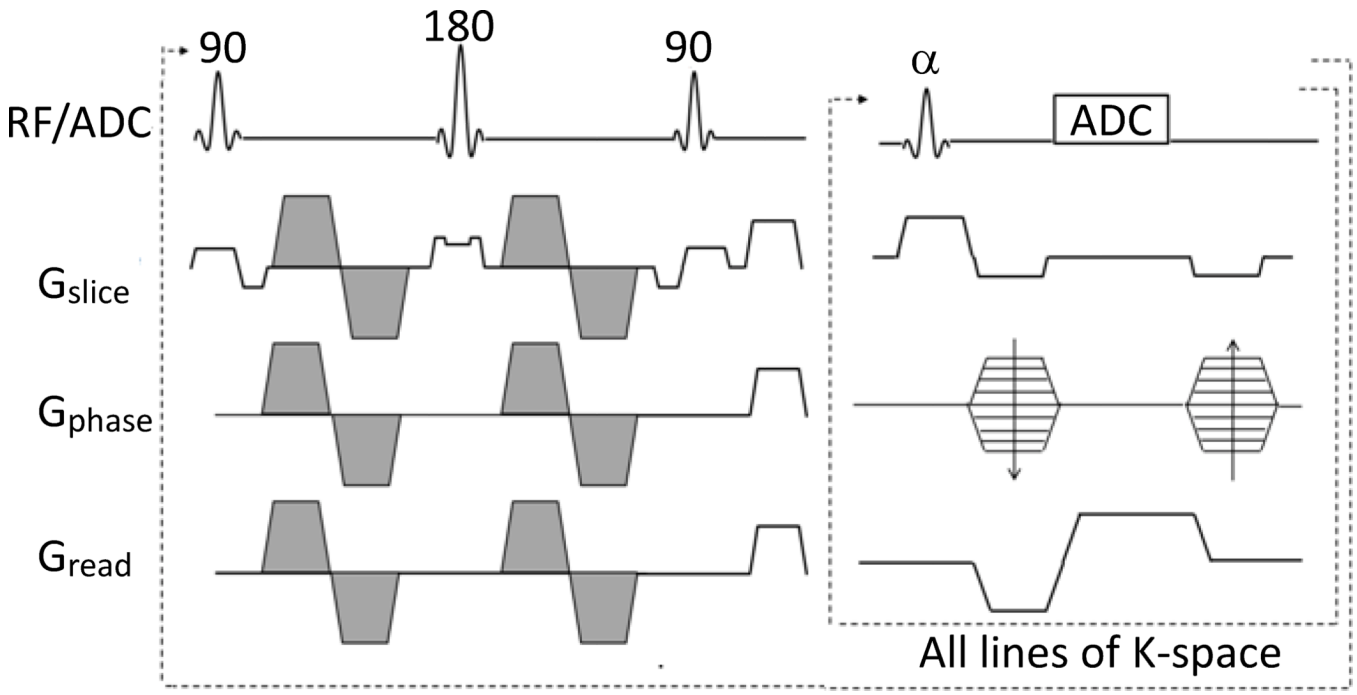

Figure 1.
Schematic of the DP-FISP pulse sequence demonstrating a single diffusion preparation with a single-shot, centrically-encoded FISP imaging readout. The diffusion weighting gradients are shaded.

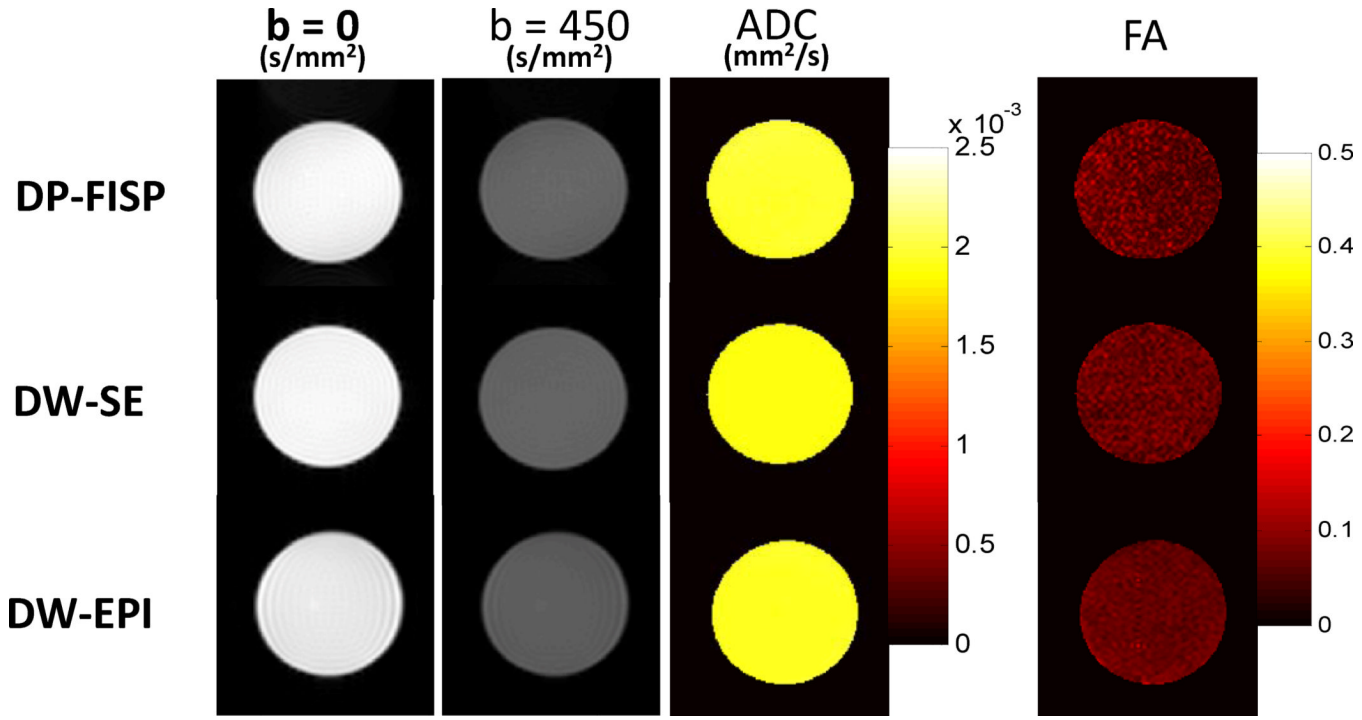

Figure 2.
Representative axial phantom diffusion weighted images, ADC, and FA maps for DP-FISP, DW-SE and DW-EPI methods (b=0 and b=450 s/mm^2, six directions). Mean values of these diffusion parameters from five repeated measurements are shown in Table 1.

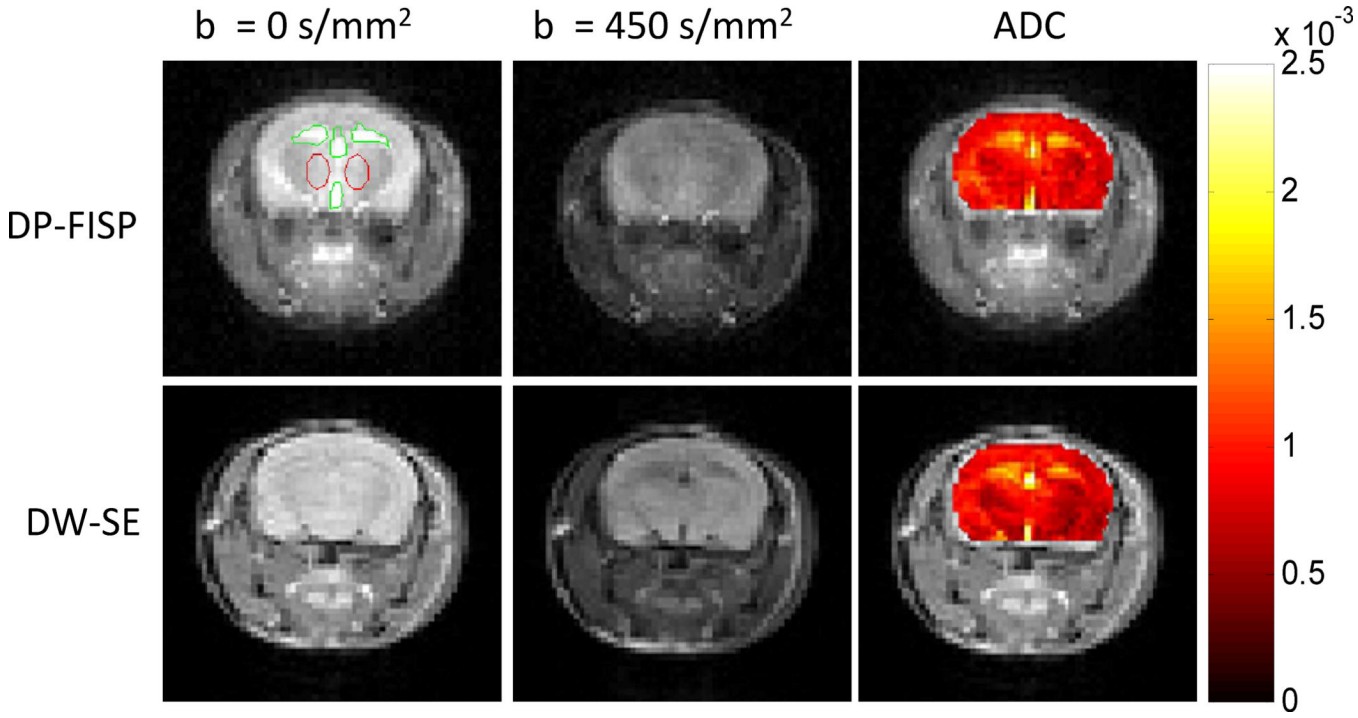

Figure 3.
Comparison of axial diffusion weighted images and corresponding ADC map (color overlay) of a mouse brain acquired using DP-FISP (4 min. acq. time) and DW-SE (40 min. acq. time). Note the good agreement of DP-FISP ADC map with the DW-SE gold standard.

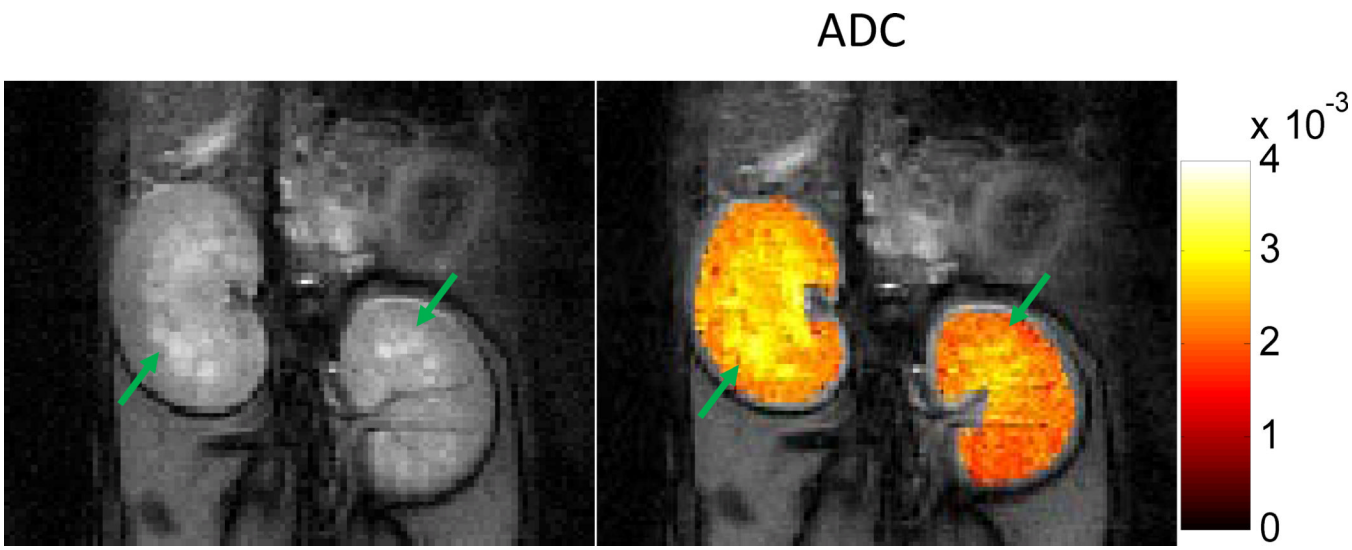

Figure 4.
Representative DP-FISP image (one average) and ADC map of a PCK rat kidney. Known renal cysts (in yellow) exhibit increased ADC values in comparison to non-cystic renal parenchyma (in red).

Table 1

Summary of phantom diffusion results for DP-FISP, DW-SE, and DW-EPI techniques.

	ADC ($\times 10^{-3}$ mm^2/s)	FA
DP-FISP	2.00±0.06	0.073±0.012
DW-SE	1.90±0.03	0.072±0.006
DW-EPI	1.97±0.04	0.070±0.007